The Vortex Lattice Method for the Wing of the Mc-Donnell Douglas F-18D Hornet

– A MATLAB implementation.

– Word Count: 1795

Rana Aymen Elsayed, ranel432
Erick Espinosa-Juarez, eries245

Linköping University
Division of Applied Thermodynamics and Fluid Mechanics
Assignment | 2022-11-21

1 Introduction

This assignment presents a MATLAB code implementing the vortex lattice method for the wing of a McDonnell Douglass F-18D Hornet. A brief descritpion of the panel methods background, motivation and methodology is first introduced. Panel visualization and lifting characteristics graphs were also generated with an added artificial dihedral angle. Finally, a discussion on the method was written along with its reach and limitations.

Figure 1: The CF-188 Hornet from the Royal Canadian Air Force. A variant of the F-18D Hornet, conserving the wing sizing analized in this assignment. [1]

1.1 Background

1.1.1 Panel Methods

Panel methods come from the necessity to better model the subsonic flow of highly sweep wings (or delta wings) where existing models such as the Traditional Prandtl's Lifting Line Model (PLLM) lose accuracy. The methodology first discretizes the surface into panels where one or more elementary flows developed from potential flow theory are attached [2]. The resulting superposition of elementary flows is a solution to the flow.Boundary conditions are placed and then the method proceeds to solve for the velocity and pressure field using equations developed for potential flow theory. The assumptions made for this method are: steady state, inviscid irrotational and attached flow For this specific project, the extra assumptions were incompressible and a thin wing.

1.1.2 The Vortex Lattice Method

The flow assigned to each of the panels in the Vortex Lattice Method (VLM) is a Horseshoe Vortex from PLLT [2]. The strenght of these vortices (their circulation Γ) is calculated for each control point (where the boundary condition is fulfiled) using the Biot-Savart Law. A set of linear equations of these circulation strenghts Γ is then solved in the way that they satisfy the boundary condition of no flow through the wing. Finally, the Kutta Joukowsky Theorem is used for solving for the lift.

1.2 Motivation

The code generated adresses the necessity to get acceptable estimations of aerodynamic properties of a modern fighter aircraft's wing in subsonic flight conditions. Also, one could say the main motivation of this assignment is to get an insight of the way aerodynamic solvers (which do not use CFD) work.

1.3 Aims

The aims of this assignment are, on the first place, the solution to a complex engineering problem using basic numerical methods but programmed from scratch. Also, to test the usage of an algorithm that models complex physical phenomena and allows to predict the aerodynamic performance of a wing. All of these while analyzing the results and making sure they are coherent to reality. Finally, by writing this assignment the communication of the results and its analysis are also presented in a formal academic way.

2 Methodology

2.1 Wing's Geometrical Parameters

The main wing's geometrical parameters for the F-18D seen in figure 2 are summarized in the folowing table:

Leading edge sweep angle [°]	Semi span [m]	Span [m]	Root Chord [m]	Tip Chord [m]	Wing Surface [m2]	Aspect Ratio [ ]	Dihedral Angle [°]
20	5.715	11.43	4.04	1.68	37.16	3.52	10*

Figure 2: F-18D Wing's geometrical parameters as reported by [3]

* Note that this angle is non-existent for the real jet, and was assigned rather arbitrary to generate a 3D problem. Besides, the flight conditions were assumed to be: airspeed $U_\infty = 20$ [m/s], air density assumed ISA at sea level $\rho = 1.225$ [kg/m3], and Angle of attack $\alpha = 1$ [rad] (althought further angle of attack evolution is presented).

2.2 General Vortex Lattice Algorithm

Because the wing is symmetric (see section 2.1) the vortex strenghts Γ were only calculated for half of the wing. Nevertheless, the contribution to induced velocities was calculated for both halves [4]. The chordwise location of the control points C for each panel ($C = r + \frac{c}{4}$) is 3/4 of a chord. To advance through the panels, the MATLAB code uses a for loop to first go through all elements in the spanwise direction and then proceeding to the next "line" in the chordwise direction. Following this, the induced velocities by the bound vortices are calculated, followed by the induced velocities of the trailing vortices. In a matrix form (which is the way it was coded in MATLAB), the sumation of these parameters is stored in the vector $\vec{V_m} = [C][\Gamma]$ with $[\Gamma]$ being a column vector of N circulations and $[C] =$

$$\begin{bmatrix} c_{1,1} & c_{1,2} & \cdots & c_N \\ c_{2,1} & c_{2,2} & \cdots & . \\ \cdots & \cdots & \cdots & . \\ c_{N,1} & c_{N,2} & \cdots & c_{N,N} \end{bmatrix}$$

Afterwards, the application of boundary conditions is done at control points (so that there is no normal flow to the surface). Finally, determination of lift force is conducted using the

Kutta-Joukowsky Theorem multiplied by two (for each wing) and getting the lift coefficient from its definition.

3 Results

3.1 General MATLAB code architecture

The attached MATLAB code follows the general procedure described previously in this section and can be seen in figure 3.

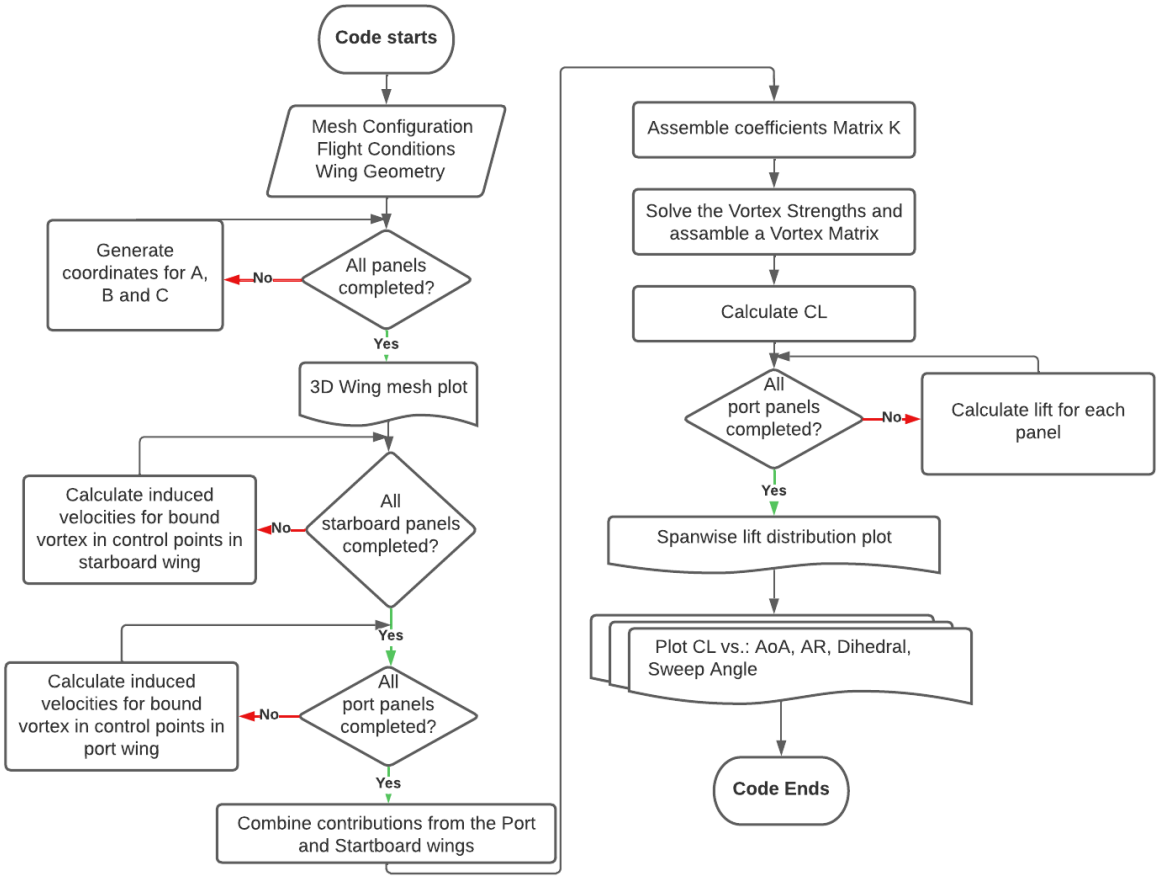

Figure 3: Flowchart of the general MATLAB architecture. Note that the script follows the logical order described previously.

The most used algorythm was the for loop, which advanced through the panels first in the spanwise direction and then in the chordwise direction. The operations coded were the cross product, matrix inversion, solving systems of equations and plot generations.

3.2 3D wing visualization

Figure 4 shows the wing for the F-18D with 2 divisions streamwise and 8 divisions spanwise (16 panels per wing in total). The bound vortex endings appear in yellow and control points in blue and the scales are both in meters.

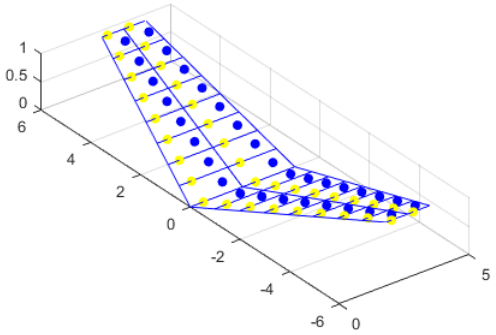

Figure 4: 3D wing visualization. The bound vortex endings appear in yellow and control points in blue.

3.3 Lift coefficient evolution plots

3.3.1 Lift coefficient vs. angle of attack

Figure 5 shows the evolution of lift coefficient C_L vs angle of attack α. Note how the expected perfectly linear beheavour of the slope, as well as a positive C_L for a zero angle of attack (eventhough the wing was not modeled cambered) and an slope close to but lower than 2π. Note that the C_L value at 1 is roughly the same as in figure 7 for $\Lambda = 20$ °.

Figure 5: C_L vs α plot. Note the expected linear beheavour and a non-zero C_L value for zero angle of attack.

3.3.2 Lift coefficient vs. sweep angle

Figure 7 shows the evolution of lift coefficient C_L vs the wing sweep angle Λ. The function shows a negative cuadratic beheavour with a maximum at around 12 ° of Λ, while the graph starts to drop sharply at around 25 °.

Figure 6: C_L vs Λ plot. A maximum occurs at around 12° and drops sharply after 25° of Λ

3.3.3 Lift coefficient vs. aspect ratio

Figure 9 shows the evolution of lift coefficient C_L vs the wing's aspect ratio . Notice the approximately but not exactly linear beheavour.

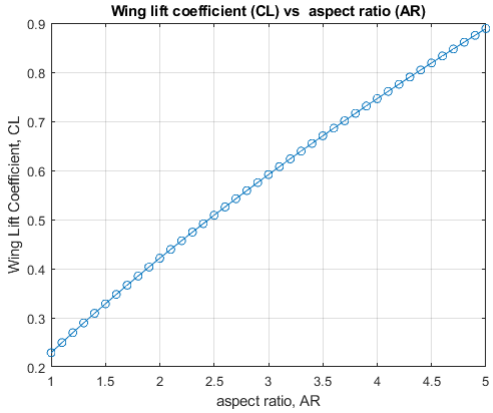

Figure 7: C_L vs AR plot. Note the tencendy of lift to increase with the aspect ratio increase.

3.3.4 Lift coefficient vs. dihedral angle

Figure 8 shows the evolution of lift coefficient C_L vs dihedral angle Φ. Note how the C_L peaks at around $\Phi = 3$ ° and becomes assymptotic to zero at around $\Phi = 25$ °.

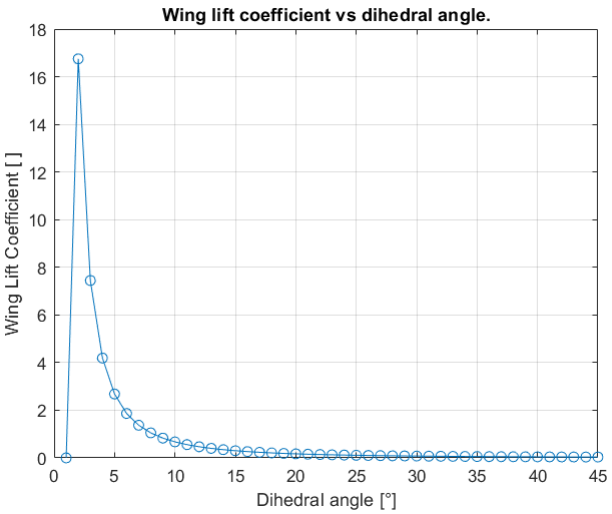

Figure 8: C_L vs dihedral angle Φ. C_L peaks at around $\Phi = 3$ °and becomes assymptotic to zero at around $\Phi = 25$ °.

It can be seen that drastic changes occur during initial variation of Φ up to 5° and an almost unuseful wing with a dihedral angle of 10°.

3.4 Spanwise distribution of the lift coecient over the wing.

Figure 9 shows the spanwise distribution of lift over the wing. Note the axis of symmetry around zero and a rather smaller slope starting from the root, reaching a peak at around 3.8 [m] and then dropping sharply.

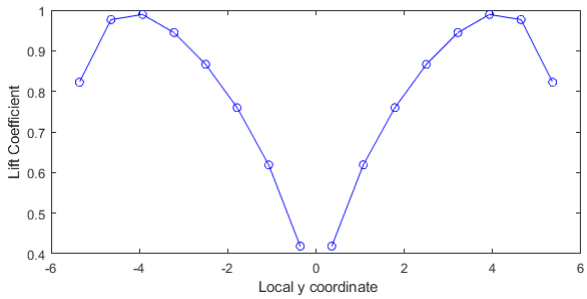

Figure 9: Spanwise distribution of lift over the wing. The symmetry around zero (x axis) is evident.

4 Discussion

The results presented in the previous section are as expected for a panel method that bases on Conventional PLLT but with some interesting findings.

4.1 Lift evolution graph discussion

The linear lift coefficient vs. angle of atack evolution (figure 5) denotes one of the principal limitations of the VLM. As stated by [2] and [5], experimentally the lift coefficient vs alpha slope only behaves linearly before boundary layer interactions become relevant enough so that complex phenomena such as recirculation, stagnation points and uneven spanwise flow end un generating boundary layer separation and eventually a stall after reaching $C_{L,max}$. Therefore, as stated in the assumptions in section 1.1.1, this model is accurate only at small angles of attack. Further discussion is needed to conclude about the existance of the non-zero lift coefficient for a zero angle of attack, as well as values above 3. The negative cuadratic-like wing lift coefficient vs sweep angle plot tendency can be explained because only the component of speed normal to the quarter-chord line of the wing is creating lift [6]. This is also the main reason why sweep wings are used in transonic airliners, because the critical reynolds number is reached at higher speeds because of this vectorial decomposition, which reduces the local angle of attack by the cosine of the sweep angle. Also, this means that the lift coefficient will always reduce compared to sweep angle, which is what happens in the figure. This means that the amount of efficient lift generated by the wing with higher Λ will always be smaller than one of a straight wing, all other conditions constant. Further discussion is needed to explain why the $C_{L,max}$ in the graph does not peak at zero but rather does it at around 10°. The lift coefficient vs. aspect rario graph (figure3) agrees with theory since higher aspect ratio wings tend to generate higher lift coefficients compared to lower AR all other variables kept constant [7]. In theory the plot continues to grow and curve until it becomes asymptotic to the C_L value corresponding to the AR $= \infty$, which would then be the lift coefficient for the two-dimensional wing [8].

Finally for this section, the lift coefficient vs. dihedral angle (figure 4) depicts a lower lifting performance of a wing the higher the dihedral angle. This makes physical sense the only velocity vector component generating lift is the one ortogonal to the wing surface (perpendicular to the flow). This means that the lift produced can be described with the equation [9]:

$$L_\Phi = L_{\Phi=0}(\cos(0) - \cos(\Phi))$$

Based on this, further discussion is needed to understand why the C_L peaks in an angle different to zero. Nevertheless, the graphs agree with the previous ecuation aftewrards since at $\approx 15^\circ$ the cosine of Φ is already 0.96.

4.2 Spanwise lift distribution discussion

The model does not have a fuselage in the middle. Figure 9 shows that the wing's lift coefficient is 0.4 at the root, which agrees to the PLLT prediction given by the following equation:

$$\Gamma(y) = \Gamma_0 \sqrt{1 - \left(\frac{y}{S}\right)^2}$$

4.3 Overall model reach and limitations

The method proves to be an efficient tool to determine overall lifting performance of the wing without the need of great computational power. This also grants flexibility to the design team since different wing configurations can be compared fast and easy (something useful during the initial conceptual design phases). The ability to have a good estimation of lifting capabilities of the wing are crucial specially during initial sizing of the airplane, and prove to be much more accurate than other simpler analytical methods.

One of the main limitations of the model is its inability to predict the drag of a lifting body or fuselage in a flow (D'Alambert Paraddox [2]). This is because as mentioned in section 1.1.1, the assumtions of inviscid flow makes the boundary layer interaction inexistant and therefore VLM predicts zero skin friction drag (since viscous flow is not modeled) and zero pressure drag (since no wake is generated by boundary layer separation or boundary layer thickening). Also, because of the limitation that the flow is attached, it gives no information on what the aeordynamic performance of the wing is during high angle of attack attitudes such as stalls and spins. These phenomena are quite complex in nature and therefore even more advanced CFD methods do not properly model this flight characteristics (unless corrections and much more simulation times are given). Besides, without further corrections of the method, compresibility at transonic speeds and hence the appearance of shock waves and expansion waves and its impact on the aerodynamic performance of the wing cannot be properly modeled. This is a huge limitation considering almost all sweep wings are designed for these speed regimes.

5 Conclusions

In the present assignment, an aerodynamic model of the wing of the F-18D Hornet was presented. The methodology was based on the vortex lattice method described extensively by [2] and resulted in the coding of a MATLAB script that generated different significant plots and results of aerodynamic performance of the wing. These graphs where further presented, described, analyzed and discussion on their results was presented. The mathematical model has an acceptable accuracy when determining lifting performance of bodies and is not that computationally or time demanding [10]. Nevertheless, as mentioned in section 4.3, the zero drag prediction of the model (consecuence of the assumtions of potential flow theory) makes it a great limitation for the aerodynamicist.

References

[1] March B, O'Malley D, Joost M. Royal Canadian Assosiation Photo Gallery (accessed 13/10/22); 2015. Available from: `https://www.rcafassociation.ca/membership/photo-gallery/`.

[2] Bertin JJ, Cummings RM. Aerodynamics for Engineers. Cambridge University Press; 2021.

[3] Boeing. Boeing F-18D Hornet (accessed 17/09/22);. Available from: `https://www.boeing.com/defense/fa-18-super-hornet/`.

[4] Gardhagen R. Introduction to Aerodynamics Class Lectures. v2022 ed. TMMV01 Course Material, Linkoping University, Sweden; 2022.

[5] Anderson, John David, Jr . Introduction to flight. 8th ed. Boston: McGraw-Hill; 2016.

[6] Liang H, Zong Z, Sun L, Zou L, Zhou L, Zhao Y, et al. Generalized Weissingerâs L-method for prediction of curved wings operating above a free surface in subsonic flow. Journal of Engineering Mathematics. 2013 12;83.

[7] Hurt, H H Jr . Aerodynamics for Naval Aviators. Reprint 1992 ed. NAVWEPS 00-80T-80, Direction of Commander, Naval Air Systems Command, United State Army, Reprint by Aviation Supplies & Academics, Inc., Rento, Washington; 1960.

[8] Luckring J. The discovery and prediction of vortex flow aerodynamics. The Aeronautical Journal. 2019 06;123:729-804.

[9] Smith HS. The Illustrated Guide to Aerodynamics. Airlife; 1992.

[10] Fearn R. Airfoil aerodynamics using panel methods. The Mathematica Journal. 2008;10(4).